Laser Diagnostics of Pulsed Corona Discharge

Ryo Ono
The University of Tokyo
Japan
ryo-ono@k.u-tokyo.ac.jp

Tetsuji Oda
The University of Tokyo
Japan
oda@ee.t.u-tokyo.ac.jp

Yoshiyuki Teramoto
The University of Tokyo
Japan
teramoto@streamer.t.u-tokyo.ac.jp

Abstract:

Laser diagnostics of atmospheric-pressure pulsed corona discharge are introduced. Density of radicals (OH, N, O, O_3, $N_2(A)$), vibrational temperature of N_2 and O_2, and translational temperature are measured in the pulsed corona discharge using laser-induced fluorescence (LIF), laser absorption, and coherent anti-Stokes Raman scattering (CARS). Their spatial profile and temporal evolution after the pulsed corona discharge are measured to study the chemical process in the postdischarge period.

1 Introduction

Pulsed corona discharge is used for pollution control and many other applications. In the corona discharge process, active species such as radicals (O, N, OH, and O_3), ions, and excited species play important roles. Measurement of these active species is indispensable for development of the corona discharge process. We have measured various active species in the pulsed corona discharge using laser-induced fluorescence (LIF), laser absorption, and coherent anti-Stokes Raman scattering (CARS). The reaction rate of these active species is affected by gas translational and vibrational temperatures. These temperatures have been also measured using the laser spectroscopic techniques. In this paper, these laser diagnostics of pulsed corona discharge are introduced. The measurements described in this paper are listed in table 1.

Table 1: Measurements of active species introduced in this paper.

Active species	Measurement method	Ref.
O_3	Absorption	[1]
OH	LIF	[2]
O	LIF	[3]
N	LIF	[4]
$N_2(A)$	LIF	[5]
NO	LIF	[6]
$O_2(v)$	LIF	[7]
$N_2(v)$	CARS	[8]
Temperature	LIF	[2]

2 Measurement

The density of active species is measured using laser absorption, LIF, and CARS. Figure 1 shows the time chart of these laser spectroscopic measurements. The laser pulse, whose pulse duration is about 20 ns, is irradiated to the plasma after an adjustable delay following the discharge pulse. The density of active species at the moment of laser irradiation is measured. By changing the delay time between the discharge pulse and the laser trigger, the temporal variation of the density after the discharge pulse is obtained.

The pulsed corona discharge occurs between a HV point electrode and a grounded plane electrode (13 mm gap length). Positive high voltage pulse is applied to the point electrode using a spark gap switch. The peak voltage is about 20 to 30 kV. Background gas flows in the discharge reactor at a rate of 2 cm/s. Typical waveforms of the discharge voltage and current are shown in Fig. 2. The discharge repetition rate is set to sufficiently low (1 pps) to reduce an accumulation of discharge byproducts in the background gas.

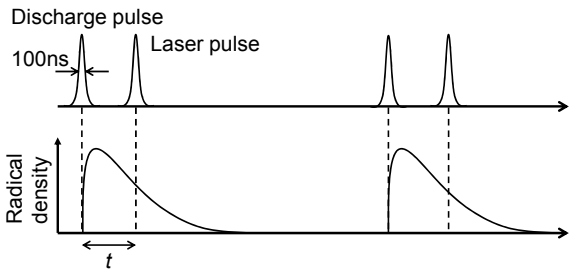

Fig. 1: Time chart of measurement.

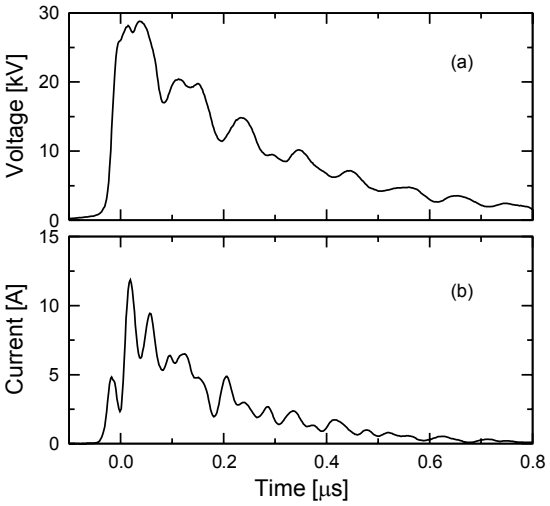

Fig. 2: Typical voltage and current waveforms.

3 Results

3.1 O_3 measurement by absorption

Figure 3 shows the time evolution of ozone density distribution after discharge pulse whose pulse duration is ~ 0.2 μs [1]. It is measured by two-dimensional laser absorption. In this measurement, a series of 25 needle electrodes with 4 mm interval is used, as shown in Fig. 3, to increase the absorption length. After the discharge pulse, ozone is produced in the postdischarge time region by $O + O_2 + M \rightarrow O_3 + M$. The increase in ozone density due to this reaction is observed in Fig. 3 for t < 100 μs. Then, ozone diffuses to ambient air for t > 1 ms.

3.2 OH measurement by LIF

OH density is measured by LIF. The setup for the LIF is shown in Fig. 4. The laser is irradiated at z mm distance from the needle tip. By varying z, one-dimensional distribution of OH density is measured. Figure 5 shows the time evolution of OH density distribution after discharge pulse [2]. At 3 μs after discharge, OH density decreases with increasing distance from the anode tip. The same tendency is also observed in ozone density (see Fig. 3). It indicates that OH and ozone are mainly produced by the secondary streamer, not by the primary streamer, as described later.

Figure 5 shows that OH density decreases with time after discharge. The decay rate near the anode tip (z < 1 mm) is much slower than that far from the anode tip (z > 1 mm). This is because the temperature near the anode tip is much higher than that far from the anode tip. OH decreases by the following reactions

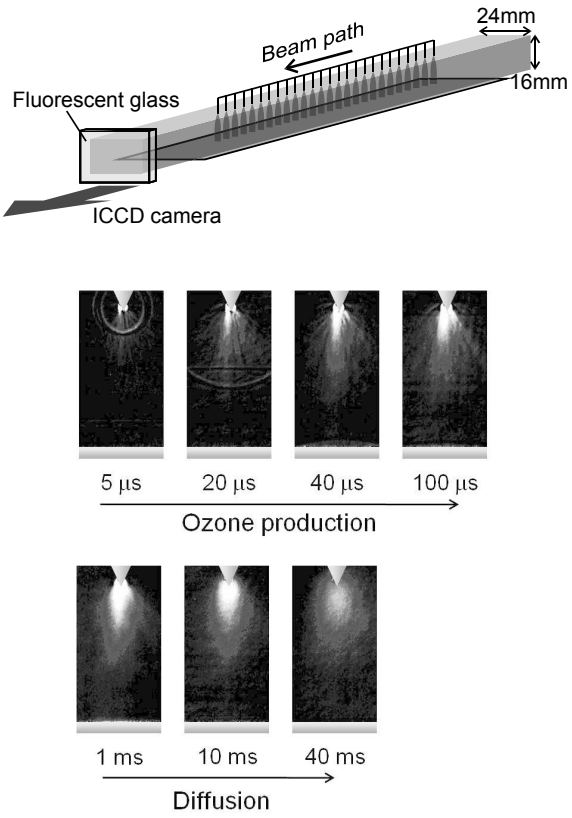

Fig. 3: Ozone density distribution measured by laser absorption (28 kV, dry air) [1]. Time represents postdischarge time.

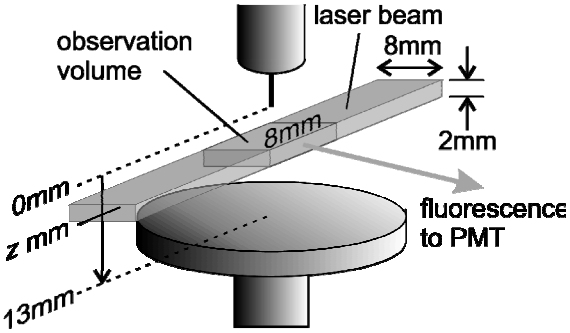

Fig. 4: LIF measurement.

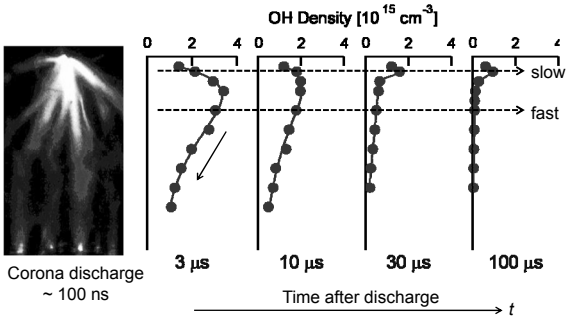

Fig. 5: Time evolution of OH density distribution after discharge [2].

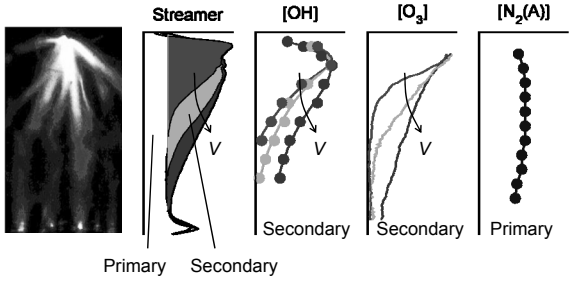

Fig. 6: Axial distributions of light emission from discharge and densities of OH, O_3, and $N_2(A)$ [1, 2, 5].

Table 2: Main production pathway of various active species by primary and secondary streamers.

Primary	$N_2(A)$, $N_2^+(B)$, $N_2(C)$
Secondary	O, N, OH, O_3, NO, $O_2(v)$, $N_2(C)$

$$OH + OH \rightarrow H_2O + O, \quad (1)$$
$$OH + OH + M \rightarrow H_2O_2 + M, \quad (2)$$
$$OH + O \rightarrow O_2 + H. \quad (3)$$

When the temperature is high, OH is produced simultaneously by

$$O + H_2O \rightarrow OH + OH, \quad (4)$$
$$H + O_2 \rightarrow OH + O. \quad (5)$$

Near the anode tip (z < 1 mm), the OH production reactions occur as well as the OH decay reactions because of high temperature.

3.3 Production of active species by primary and secondary streamers

Figure 6 shows the axial distributions of light emission from the discharge and densities of some active species [1, 2, 5]. They are plotted for various discharge voltages V. The results are properly normalized. The colored areas in the streamer emission having negative slope are emission from the secondary streamer, while the non-colored areas having flat profile are emission from the primary streamer [9]. The OH and O_3 profiles are similar to the secondary streamer emission profile, while $N_2(A)$ profile is similar to the primary streamer emission profile. It indicates that OH and O_3 are mainly produced by the secondary streamer, while $N_2(A)$ is mainly produced by the primary streamer. In this way, the main production pathway of active species can be analyzed using the axial distribution of their densities. Table 2 summarizes the main production pathway of various active species by primary and secondary streamers.

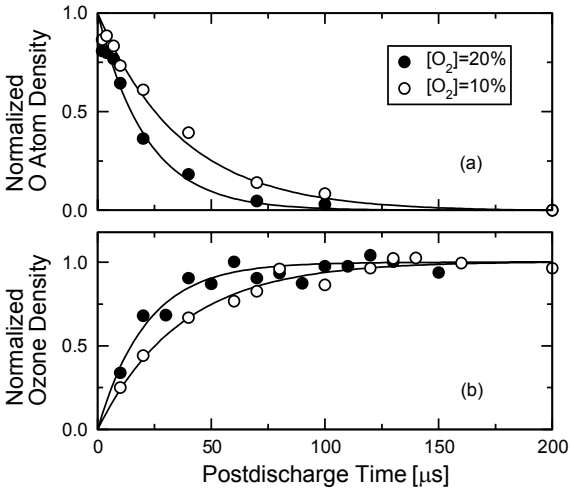

Fig. 7: Time evolution of O and O_3 densities after discharge in O_2/N_2 [3]. The results are properly normalized.

3.4 Time evolution of densities of active species after discharge

3.4.1 O radical and O_3

In dry air condition, O radicals produced by the discharge mostly react with O_2 to produce O_3 in the postdischarge period

$$O + O_2 + M \rightarrow O_3 + M. \quad (6)$$

Therefore, the decay rate of O is equivalent with the increasing rate of O_3, as shown in Fig. 7 [3]. The time constant of the decay of O and the increase in O_3 is 10 to 100 μs in the O_2/N_2 mixture.

In humid air, O radical also decreases by

$$O + OH \rightarrow O_2 + H, \quad (7)$$
$$O + H_2O \rightarrow OH + OH. \quad (8)$$

Therefore, O density decreases faster than that in dry air [10].

3.4.2 OH radical

OH decreases by recombination reactions (1) and (2). Therefore, the rate of OH decay after discharge is faster at higher OH density. In addition, it is faster at higher O_2 concentration because OH reacts with O radical as reaction (3) [11]. The decay time constant of OH is 10 μs to 1 ms in usual pulsed corona discharge.

3.4.3 N radical

N radical decreases by recombination reaction in N_2 discharge

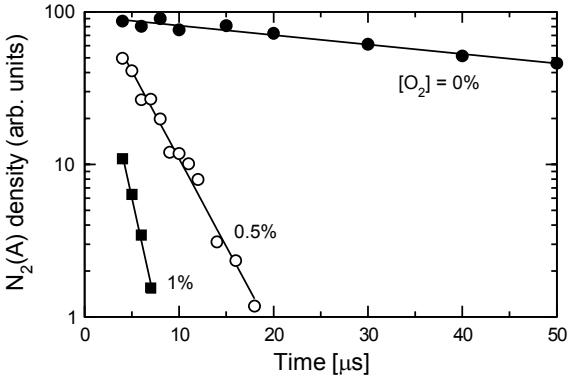

Fig. 8: Decay of N_2(A) density after discharge in O_2/N_2 for various O_2 concentrations [12].

$$N + N + M \rightarrow N_2 + M. \quad (9)$$

Its decay rate depends on N density. That is, the absolute N density can be obtained from its decay rate after discharge. For example, the N density immediately after discharge (t = 0 μs) is 500 ppm at z = 0.5 mm when V = 21.5 kV [4].

In O_2/N_2 discharge, N radicals also reacts with O_2

$$N + O_2 \rightarrow NO + O, \quad (10)$$

and NO produced in discharge

$$NO + N \rightarrow N_2 + O. \quad (11)$$

Therefore, the decay rate of N density after discharge increases with O_2 concentration.

3.4.4 N_2(A) metastable

N_2(A) rapidly reacts with O_2

$$N_2(A) + O_2 \rightarrow N_2 + O + O. \quad (12)$$

The decay rate of N_2(A) is strongly affected by O_2 concentration, as shown in Fig. 8 [5, 12]. In N_2 discharge, its density can be obtained from its decay rate after discharge since N_2(A) decreases by recombination reaction. The N_2(A) density in N_2 discharge is less than 10 ppm at z = 6 mm when V = 21.5 kV [5]. It appears to be smaller than the densities of other active species such as O, N, OH, and O_3.

3.5 Observation of NO removal

NO removal by the discharge is measured. Figure 9 shows the NO removal after pulsed dielectric barrier discharge in NO(200 ppm)/N_2 [6]. It is observed by two-dimensional LIF. It is observed that NO is removed by reaction with N radicals (11) in the postdischarge period.

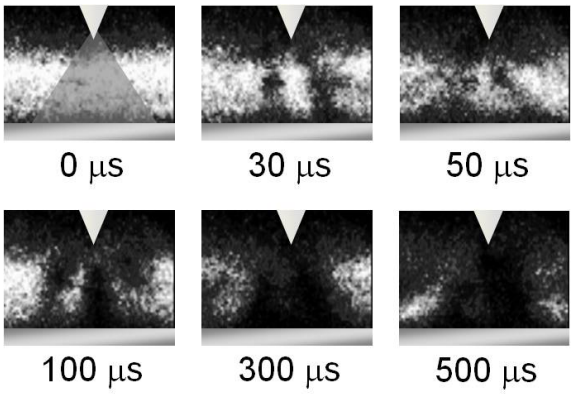

Fig. 9: NO removal by pulsed dielectric barrier discharge in NO(200 ppm)/N_2 [6]. V = 25 kV.

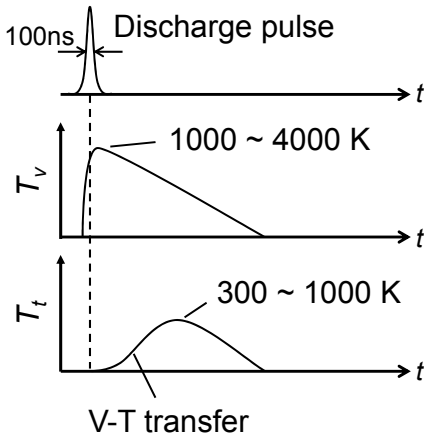

Fig. 10: Time evolution of vibrational temperature T_v and translational temperature T_t.

4 Vibrational and translational temperatures

4.1 Vibrational temperature

In the pulsed corona discharge, most of the electron energy is used to increase the vibrational temperature, and only a small proportion of the electron energy is used to increase the gas temperature. As a result, the vibrational temperature is much higher than the gas temperature. After the discharge pulse, the vibrational temperature decreases and energy is released to the ambient gas. This released energy heats the ambient gas, leading to an increase in gas temperature in the afterglow of the discharge pulse (Fig. 10) [13, 14]. Because the gas temperature strongly affects the rate of chemical reactions, the rate of the vibration-to-translation (V–T) energy transfer is an important factor in plasma kinetics.

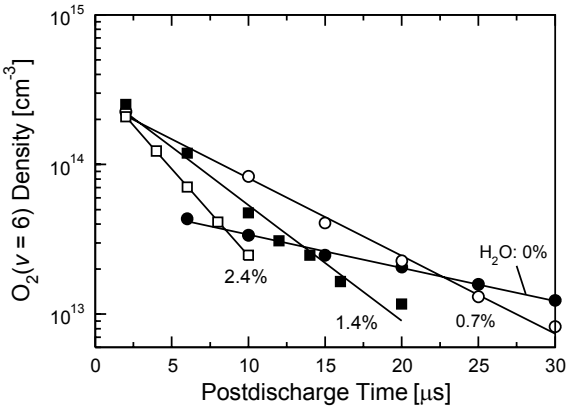

Fig. 11: Time evolution of O(v = 6) density after discharge in dry and humid air [7].

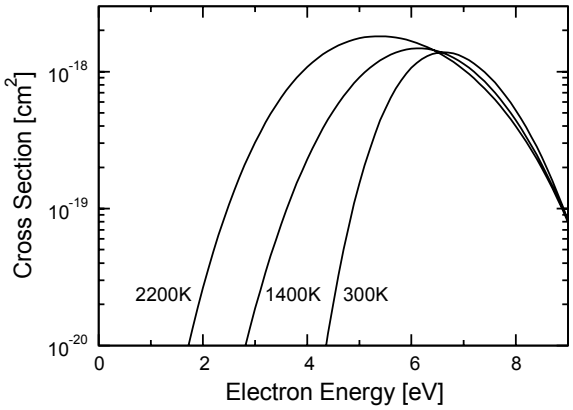

Fig. 12: Calculated cross section of dissociative attachment (12) for T_r = T_v = 300, 1400, and 2200 K [16]. It is obtained from table 1 in [17].

Figure 11 shows the decay of $O_2(v = 6)$ after discharge in dry and humid air measured by LIF [7]. It shows the decrease in $T_v(O_2)$ by the V-T energy transfer process. Similarly, it is observed by CARS that $T_v(N_2)$ also decreases after discharge by the V-T process [15]. Figure 11 shows that the V-T energy transfer is faster at higher humidity. This is due to the unique characteristics of H_2O molecules related with V-T energy transfer process[7].

The vibrational temperature has another important factor. The cross section of dissociative attachment

$$e + O_2 \rightarrow O^- + O, \qquad (12)$$

strongly depends on vibrational temperature. An example is shown in Fig. 12 [16, 17]. The slight increase in $T_v(O_2)$ (300 → 2200 K) leads to remarkable decrease in the threshold electron energy required for the dissociative attachment of O_2. It indicates that $T_v(O_2)$ markedly affects the production of active species (O and O^-), particularly for low electron energy.

4.2 Translational temperature

Due to the V-T energy transfer process, translational temperature increases after discharge pulse. The rise in temperature after discharge is measured by OH LIF, where OH rotational temeprature is assumed to be equivalent to translational temperature. Figure 13 shows the results [2]. It shows that temeprature increases after discharge, particularly near the anode tip. Due to this non-uniform distribution of temperature, the chemical reaction near the anode tip is different from other region, as shown in Fig. 5.

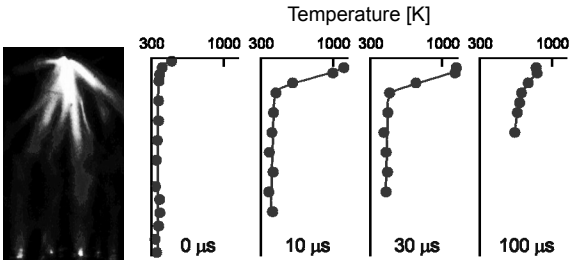

Fig. 13: Time evolution of temperature distribution after discharge in $H_2O(2.8\%)/O_2(2\%)/N_2$ measured by OH LIF [2]. V = 32 kV.

The rise in temperature shown in Fig. 13 causes a decrease in ambient gas density in the streamer channel after discharge. It can be quantitatively observed by shadowgraph [18]. The spot heating near the anode tip shown in Fig. 13 generates a spherical pressure wave centered on the anode tip. It can be observed by schlieren method (Fig. 14) [19].

5 Conclusions

Laser diagnostics of pulsed corona discharge were introduced. The production of various active species (O, N, OH, O_3, NO, O_2(v), N_2(A), N_2(C), N_2^+(B)) by the primary and secondary streamers and the time evolution of their densities after discharge were described. The vibrational and translational temperatures were also measured. The decrease in vibrational temperature and the increase in translational temperature after discharge due to V-T energy transfer process were measured. The effect of vibrational temperature on the electron collision process was described.

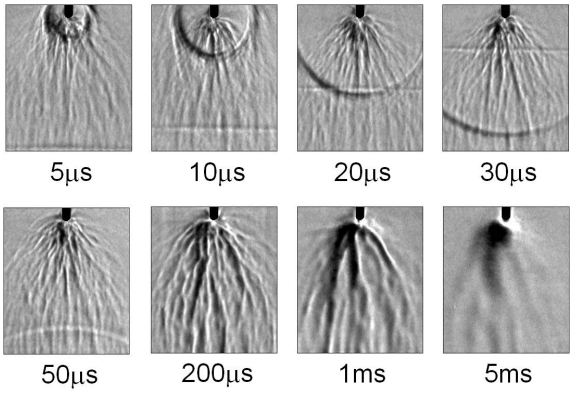

Fig. 14: Schlieren images of pressure wave and streamer channels in humid air discharge [19]. V = 26 kV.

References

[1] R. Ono and T. Oda; "Spatial distribution of ozone density in pulsed corona discharges observed by two-dimensional laser absorption method," J. Phys. D, **37**, pp. 730-735 (2004).

[2] R. Ono and T. Oda; "Measurement of gas temperature and OH density in the afterglow of pulsed positive corona discharge," J. Phys. D, **41**, 035204 (2008).

[3] R. Ono, K. Takezawa and T. Oda; "Two-photon absorption laser-induced fluorescence of atomic oxygen in the afterglow of pulsed positive corona discharge," J. Appl. Phys., **106**, 043302 (2009).

[4] R. Ono, Y. Teramoto and T. Oda; "Measurement of atomic nitrogen in N_2 pulsed positive corona discharge using two-photon absorption laser-induced fluorescence," Jpn. J. Appl. Phys., **48**, 122302 (2009).

[5] Y. Teramoto, R. Ono and T. Oda; "Measurement of N_2(A) metastable in N_2 pulsed positive corona discharge with trace amounts of additives," J. Phys. D, **42**, 235205 (2009).

[6] R. Ono and T. Oda; "Optical diagnosis of pulsed streamer discharge under atmospheric pressure," Int. J. Plasma Environ. Sci. Technol., **1**, pp. 123-129 (2007).

[7] R. Ono, Y. Teramoto and T. Oda; "Effect of humidity on gas temperature in the afterglow of pulsed positive corona discharge," Plasma Sources Sci. Technol., **19**, 015009 (2010).

[8] K. Tanaka, Y. Teramoto, R. Ono and T. Oda; "Measurement of vibrational temperature in the afterglow of atmospheric positive corona discharge using BOX-CARS," 34th annual meeting of IESJ, pp. 201-204, (2010) (in Japanese).

[9] R. Ono and T. Oda; "Formation and structure of primary and secondary streamers in positive pulsed corona discharge — Effect of oxygen concentration and applied voltage," J. Phys. D, **36**, pp. 1952-1958 (2003).

[10] R. Ono, Y. Yamashita, K. Takezawa, and T. Oda; "Behavior of atomic oxygen in pulsed dielectric barrier discharge measured by laser-induced fluorescence," J. Phys. D, **38**, pp. 2812-2816 (2005).

[11] R. Ono and T. Oda; "Dynamics of ozone and OH radicals generated by pulsed corona discharge in humid-air flow reactor measured by laser spectroscopy," J. Appl. Phys., **93**, pp. 5876-5882 (2003).

[12] R. Ono, C. Tobaru, Y. Teramoto and T. Oda; "Observation of N_2(A) metastable in pulsed positive corona discharge using laser-induced fluorescence," IEEE Ind. Applicat. Conf. 43th IAS Annual Meeting, Edmonton, 12P-7 (2008).

[13] G. Hartmann and I. Gallimberti; "The influence of metastable molecules on the streamer progression," J. Phys. D, **8**, pp. 670-680 (1975).

[14] O. Eichwald, M. Yousfi, A. Hennad and M. D. Benabdessadok; "Coupling of chemical kinetics, gas dynamics, and charged particle kinetics models for the analysis of NO reduction from flue gases," J. Appl. Phys., **82**, pp. 4781-4794 (1997).

[15] R. Ono, A. Komuro, Y. Nakagawa, Y. Teramoto and T. Oda; "Vibrational and translational temperature in the afterglow of pulsed positive corona discharge," Int. Conf. Gas Discharges and Their Applicat., Greifswald, pp. 228-231 (2010).

[16] R. Ono and T. Oda; "Measurement of vibrationally excited $O_2(v = 6)$ in the afterglow of pulsed positive corona discharge," Plasma Sources Sci. Technol., **18**, 035006 (2009).

[17] T. F. O'Malley; "Calculation of dissociative attachment in hot O_2," Phys. Rev., **155**, pp. 59-63 (1967).

[18] R. Ono, Y. Teramoto, and T. Oda; "Gas density in pulsed positive streamer measured by laser shadowgraph," J. Phys. D, **43**, 345203 (2010).

[19] R. Ono and T. Oda; "Visualization of streamer channels and shock waves generated by positive pulsed corona discharge using laser schlieren method," Jpn. J. Appl. Phys., **43**, pp. 321-327 (2004).